

Microfabricated Near-field Scanning Microwave Probes

Yaqiang Wang and Massood Tabib-Azar

Department of Electrical Engineering and Computer Science
Case Western Reserve University, Cleveland, Ohio 44106
(e-mail: tabib-azar@po.cwru.edu)

Abstract

Design, microfabrication and characterization of co-axial microwave tips compatible with commercial atomic force microscope (AFM) are discussed. Simultaneous microwave and AFM images of materials, cells and devices, obtained using these tips, reveal interesting "inner" structures undetectable using AFM alone. The near-field microwave co-axial tips are capable of performing measurements both in reflection (R) and transmission (T) modes. R/T capability enable them to map the microwave conductivity/permittivity of objects or image electromagnetic near-field radiation patterns near active devices or through various objects over a wide frequency range of 0.5-20 GHz with possible extensions up to 100 GHz.

Introduction

Local scanning probes such as scanning tunneling (STM), scanning capacitance (SCM), near-field scanning optical (NSOM), and atomic force microscopes (AFM) have become important tools in imaging of materials with near atomic resolution [1]. These probes, however, either operate with low frequency signals (≤ 1 GHz) or they operate in the optical regime (figure 1). The purpose of the present study was to design and fabricate co-axial near-field microwave probes [2-8] compatible with AFM, to bridge the frequency gap that currently exist in local probe microscopy.

Applications of near-field scanning microwave imaging (NSMI) probes are far reaching and include novel magnetic resonance imaging with very high spatial resolution and 3-D imaging of organic molecules [9]. Scanning microwave probes are also suitable for nondestructive surface imaging and subsurface characterization of materials over a wide frequency range.

In the device research areas, the NSMI can be used to map the microwave properties of various regions of a device under the actual operation conditions with parameters including operation frequency and dc biasing. In the biological areas, the penetration of microwave signal inside cells or other relevant biological materials, enable imaging organelles and internal structures that remain undetectable in topographical AFM imaging or scanning electron microscopy (SEM) that owing to its 5-30 kV electron energy damages the structure during imaging. Non-ionizing, low energy NSMI enables imaging these internal structures without damaging the delicate membranes and tissues and inside buffer solutions.

The present work describes design, fabrication and characterization of AFM-compatible near-field co-axial microwave probes. The ability to perform microwave and AFM measurements simultaneously is quite valuable and it enables AFM topographical images to provide a reference landscape to understand and interpret the microwave images. The AFM standoff compensation mechanism also enables construction of microwave images that truly reflect the microwave property maps avoiding standoff artifacts.

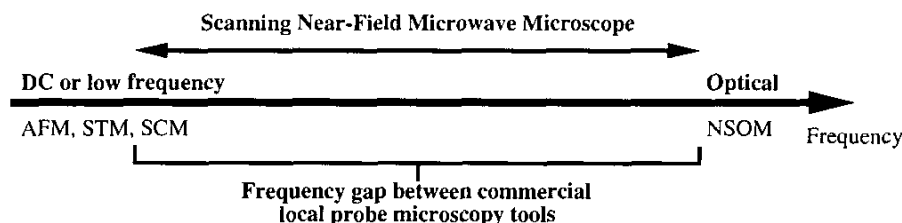


Figure 1 Frequency spectrum for different scanning techniques. STM, AFM and related techniques (such as MFM, SCM, etc.) all operate near dc and below 1 GHz. Between these techniques and NSOM there is a very large frequency gap. The scanning near-field microwave microscopy fills this gap and provides a method to image the complex permittivity function of materials, devices and biological objects.

Near-Field Microwave Co-axial Probes

Design. Dimensions, and the probe tip geometry were all chosen to yield cantilever beams compatible with commercial AFM tips [5]. Rectangular as well as V-shaped beams (see figure 1) were designed. The effective Hooke's constants in the range of 0.1-10 N/m were targeted resulting in resonant frequencies of 10-100 KHz.

The waveguide had a co-planar geometry over the V-shaped beam arms that connected $100 \times 100 \mu\text{m}^2$ pads to the co-axial tip with conical shape. The co-planar section was designed to have 50Ω characteristic impedance. The $10\text{-}\mu\text{m}$ high co-axial conical tip region was designed to have a very narrow opening of around 100 nm to expose a tip apex of around 10-nm apex.

Fabrication. The starting substrate was a 4-inch double side polished silicon on insulator (SOI) wafer with 10-15 μm device layer, 1 μm buried oxide layer, and a 400 μm handle layer. Both the Si device layer and the handle layer were p-type with (100) orientation. Over 300 probe chips were fabricated per wafer. The main fabrication steps are shown in figure 2.

After a RCA cleaning step, the SOI wafer was thermally oxidized in the furnace at temperature of 1200 $^{\circ}\text{C}$ to grow 1 μm thick SiO_2 film. The photolithography #1 defined circular patterns for Si tip etching. Next, the exposed thermal oxide was etched away by buffered oxide etch (BOE). Then, plasma etching was performed to form conical Si tips. SF_6 was the main etching gas to undercut the oxide-resist mask to form blunt conical silicon tips (figure 2a, also see figure 3a for SEM photo).

Si tips ($\sim 10 \text{ nm}$) were then obtained (figure 3b) using thermal oxidation sharpening method. The mechanism is based on oxidation inhibition at regions of high curvature. The growth rate at the apex of the tips is lower than other regions. Therefore, Si tips become sharper after thermal oxide removal [5]. Next, photolithography #2 exposed tip regions that were made conductive by a boron ion implantation. The ion implantation was performed with a dose of 5×10^{16} ions/ cm^2 at 60 KeV (figure 2b). The aluminum waveguide formed ohmic contact to these highly conductive tips.

To form the waveguide (see figure 3d for SEM photo), a 5000 \AA -thick aluminum was sputtered at the pressure of 1×10^{-7} Torr. The metal waveguide was defined by photolithography #3 and patterned by aluminum wet etch (figure 2c). Low-pressure chemical vapor deposition (LPCVD) was then used to deposit a 3000 \AA layer of low temperature oxide (LTO) at 450 $^{\circ}\text{C}$ and at 350 mTorr. The 3000 \AA LTO layer acted as an isolation layer between the metal waveguide and the co-axial metal shield layer at the tip region (figure 2d). Next, a 1-2 μm layer of aluminum was sputtered and patterned by photolithography #4 to form a metal shield layer. Photolithography #5 was used to pattern the LTO layer

after wet etching of the metal to expose the underneath metal waveguide (figure 2e and figure 2f).

Co-axial Tip Formation. A "tip exposure" step was developed and used to open the top aluminum layer over the sharpened Si apex to form a co-axial tip (see figure 3c for SEM photo). First, thick (8-10 μm) photoresist AZ 9260 was spun to achieve uniform coating on the wafer. Next, a photoresist plasma stripper M4L was utilized to etch photoresist to the extent that the aluminum coated tip was barely exposed. The tip exposure was controlled by tuning the parameters of the plasma photoresist stripper. The aperture in the aluminum shield layer was opened using metal wet etch. Then, the conductive bare Si tip was exposed by a LTO etch step to achieve the co-axially shielded tip structure (figure 2g). The photoresist was removed before a new layer of thick photoresist was coated to protect the co-axial tip in the next photolithography step.

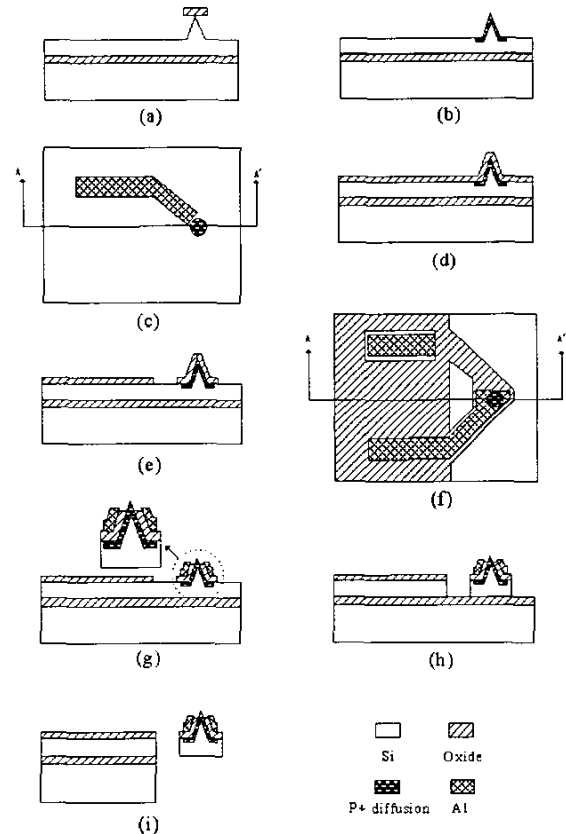


Figure 2 Process flow of the probe fabrication. See the text for explanation of important steps shown here.

Si anisotropic plasma etch was done after photolithography #6 to form a V-shaped cantilever beam thickness of 5 μm (figure 2h also see figure 3d for SEM photo). Thick photoresist was spun again to protect the front side of the device layer before the backside of the handle layer goes to the last photolithography step.

Double side alignment was used to define the backside DRIE region to release the V-shaped cantilever beam. The exposed backside Si regions were etched in a DRIE system from STS (Gwent, UK) until reaching the buried oxide layer. This system provided etching selectivity between Si and SiO₂ of 150:1, and selectivity between Si and photoresist of 75:1. Finally, the microwave probe was released by oxide etch and photoresist strip (figure 2i).

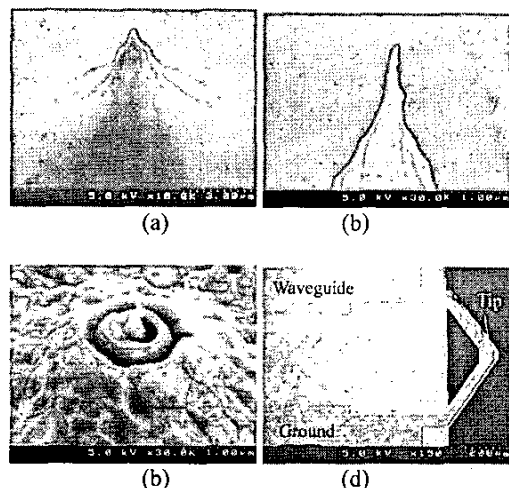


Figure 3 SEM photos of the fabricated co-axial tip. (a) Conical silicon tip. (b) Conical silicon tip after oxidation sharpening. (c) Co-axially shielded silicon tip. (d) The released V-shaped silicon beam with co-axial tip.

Characterization. A commercially available AFM platform was used for the measurement of the properties of the micro-fabricated microwave probe. Figure 4 shows the normalized mechanical oscillation spectrum of our fabricated probe. For comparison, we have also included the oscillation spectrum of a commercially available non-contact metallic tip. The quality factor of our resonator is 3 time better and its other mechanical parameters are: effective Young's modulus ≈ 1550 GPa, Hooke's constant ≈ 1 N/m, and resonant frequency ≈ 100 KHz.

The electrical characterization was performed using a HP 8721C network analyzer to measure the input reflection coefficient S_{11} with and without a sample near the tip. Figure 5 shows the reflection (S_{11}) spectra of our tip in air and over a metallic sample. The tip was designed to have 50 Ω characteristic impedance around 2 GHz.

Microwave/AFM Images. Results using simultaneous AFM and microwave imaging at 1-20 GHz to study internal structures in biological cells is shown in figure 6. It can be seen that the cell nuclei can be easily

detected under cell membrane using the microwave signal while the AFM image only reveals the cell topography. The spatial resolution of the probe at 1.8 GHz was around 10 nm and its permittivity resolution ($\Delta\epsilon/\epsilon$) was around 10^{-3} .

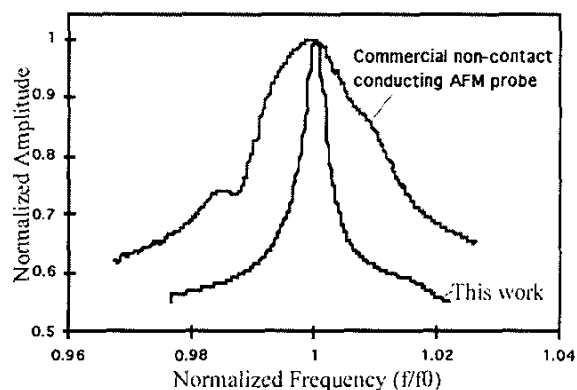


Figure 4 Normalized mechanical oscillation spectrum.

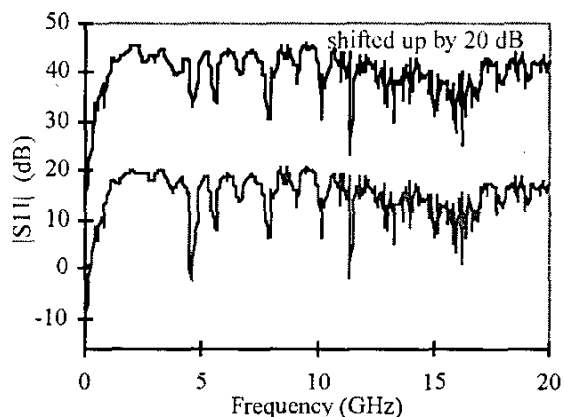


Figure 5 Reflection ($|S_{11}|$) spectra of tip in air (top) and over a metallic sample (bottom). There is a large sensitivity to the metallic (Au) sample around 5 GHz. Transmission spectra was also obtained but not shown here.

Currently we are in the process of designing our third generation tips with asymmetric stripline waveguide geometry to shield the arms of the probe from sample. We are also experimenting with carbon-nanotubes grown over the tip apex as shown in figure 7. This approach has the advantage of providing sharper tips (single wall carbon nanotubes have diameter as small as 3 nm) and tips grown in a trench that may contain the terminal point of the active waveguide. This can be used to achieve smaller aperture with simplified fabrication steps.

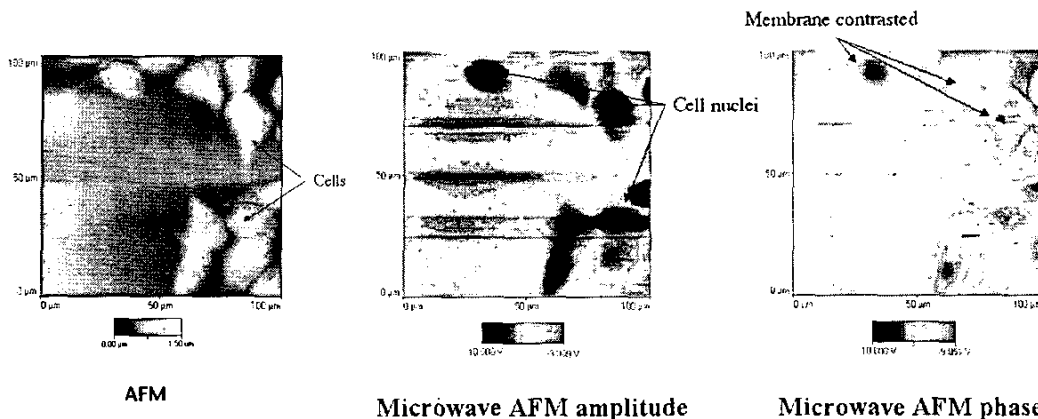


Figure 6 AFM and reflected microwave/AFM images of breast cancerous cells grown on a glass substrates. The AFM image shows topography of the cell. The microwave images (1.8 GHz) show both the dense cell nuclei and the membrane contours depending on whether the amplitude or phase signal is used.

Moreover, carbon nanotubes [10] probably offer the best and highest frequency mechanical resonators for a variety of applications including chemical sensing (micro-balance) and communication (mechanical filters, etc.).

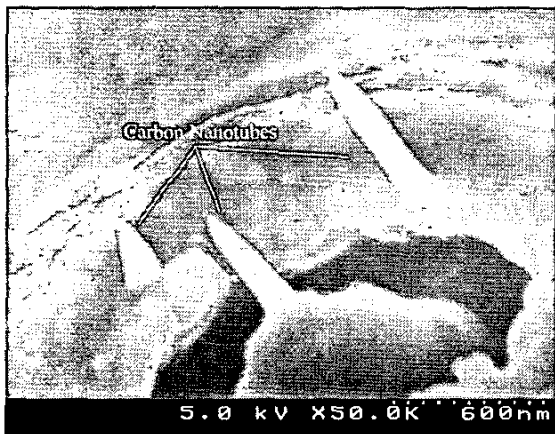


Figure 7 Carbon nanotubes grown over the co-axial tip.

We acknowledge supports from AFOSR, NSF and NIST and contributions from Mr. T. Zhang (figure 6) and Mr. L. You (figure 7).

References

1. G Binnig, C.F. Quate, "Atomic Force Microscope." *Phys. Rev. Lett.* 56, pp. 930-933 (1986).
2. M. Tabib-Azar, N. Shoemaker and S. Harris, "Nondestructive Characterization of Materials by Evanescent Microwaves." *IOP Meas. Sci. & Tech.*, Vol. 3, pp. 583-590 (1993).
3. M. Tabib-Azar, J. L. Katz, S. LeClair, "Evanescent Microwaves: A Novel, Super-resolution, Noncontact and Nondestructive Imaging Technique for Biological Applications." *IEEE Trans. on Instr. and Meas.*, pp. 1111-1118 (1999).
4. M. Tabib-Azar and S. R. LeClair, "Applications of Evanescent Microwave Probes in Gas and Chemical Sensors." *Sens. and Act. B* 67, pp. 112-121 (2000).
5. Y. Wang and M. Tabib-Azar, "Fabrication and Characterization of Evanescent Microwave Probes Compatible with Atomic Force Microscope For Scanning Near-Field Microscopy." *Proceedings of 2002 ASME Inter. Mech. Eng. Congress & Expo.*, New Orleans, Louisiana, November 17-22 (2002).
6. M. Tabib-Azar, "Near-Field Scanning Microwave Microscopy of Molecules and Compliant Substrates." *Proceedings of 11th Int. Con. on STM and Related Tech.*, Univ. of British Columbia, Vancouver, Canada, p.179, July 12-20 (2001).
7. M. Tabib-Azar, J. L. Katz, P. Spencer, A. Scott, Y. Wang, "Acousto-Opto-Electromagnetic Properties of Human Dentin and Cortical Bone Collagen." *Proceedings of the 46th Mtg. of Biophys. Soc.*, San Francisco, p. 513a (2002).
8. B. T. Rosner and D. W. van der Weide, "High-Frequency Near-Field Microscopy." *Rev. of Sci. Instr.*, Vol. 73 (7), pp. 2505-2525 (2002).
9. J.A. Sidles, J. L. Garbini, and G. P. Drobny, "The Theory of Oscillator-Coupled Magnetic Resonance with Potential Applications to Molecular Imaging." *Review of Scientific Instruments*, Vol. 63 (8), pp. 3881-3899 (1992).
10. S.B. Sinnott and R. Andrews, "Carbon Nanotubes: Synthesis, Properties, and Applications." *Critical Reviews in Solid State and Mater. Sc.*, Vol. 26 (3), pp. 145-249 (2001).